J Fail. Anal. and Preven. (2021) 21:738–746
https://doi.org/10.1007/s11668-021-01143-5

CASE HISTORY—PEER-REVIEWED

Keystone Pipeline Rupture Investigation

Matthew R. Fox · Adrienne V. Lamm

Submitted: 4 February 2021 / Accepted: 8 March 2021 / Published online: 27 March 2021

Abstract The National Transportation Safety Board coordinated with the Pipeline and Hazardous Materials Safety Board to investigate the November 16, 2017, rupture of Keystone Mainline number 1 crude oil pipeline operated by TransCanada Oil Pipeline Operations, Incorporated. The rupture resulted from a fatigue crack that initiated from near-surface cracks associated with sliding contact damage at the top of the pipe and propagated to failure within 7.4 years of pipeline operation. The surface damage was characterized by photography, scanning electron microscopy, energy-dispersive x-ray spectroscopy, metallography, and dimensional analyses, and findings indicated the damage was produced by contact with a steel component likely from a vehicle used during the original construction after the pipeline was positioned in the trench.

Keywords Crude oil pipeline · Fatigue cracking · Construction damage · Near-surface cracks · Keystone

Introduction

On November 16, 2017, the Keystone Mainline number 1 pipeline operated by TransCanada Oil Pipeline Operations, Incorporated (TransCanada), ruptured near Amherst, South Dakota, releasing an estimated 6592 barrels of crude oil (Fig. 1). The National Transportation Safety Board (NTSB) coordinated with the Pipeline and Hazardous Materials Safety Administration (PHMSA) to examine the pipe at the NTSB Materials Laboratory facilities in Ashburn, Virginia, and Washington, DC. This article will focus on the examinations conducted by the NTSB Materials Laboratory in support of the failure investigation. Additional information about the overall investigation, findings, and conclusions is presented in NTSB Pipeline Accident Brief PAB-18/01 and PHMSA Failure Investigation Report: Material Failure—Mechanical Damage from Original Construction—TC Oil Pipeline Operations, Inc. [1, 2]. Additional details of the NTSB Materials Laboratory examination are presented in Materials Laboratory Factual Report 18-017 [3].

The Keystone pipeline had been in operation for 7.4 years at the time of the rupture. The ruptured segment was a 30-in. (76.2-cm)-diameter pipe with a 0.386-in. (9.80-mm) nominal wall thickness and a double submerged arc welded (DSAW) longitudinal seam. Manufactured in 2008 by Berg Steel Pipe Corporation (Panama City, Florida), the pipe steel was certified to American Petroleum Institute (API) Specification 5L Grade X70 product specification level (PSL) 2 with a fusion-bonded epoxy (FBE) coating [4]. Concrete set-on weights, used to keep the pipeline from floating to the surface in wet environments, were installed over the pipeline near the rupture. Records at the pump station located 17 miles (27 km) upstream of the rupture location indicated the rupture occurred during an anticipated gradual pressure increase associated with bypass operations at the downstream pump station. The discharge pressure at the upstream pump station remained below the maximum operating pressure of 1440 psig (99.3 bar) for the ruptured segment. A 9-foot 10-in. (3.00-m)-long section of the pipe containing the 4-foot 4-in. (1.32-m)-long rupture was sent to the NTSB Materials Laboratory for further examination (Fig. 2).

M. R. Fox (✉) · A. V. Lamm
Materials Laboratory Division, National Transportation Safety Board, 490 L'Enfant Plaza East, SW, Washington, DC 20594, USA
e-mail: FOXM@ntsb.gov

Fig. 1 Aerial view of the accident site *Source*: https://twitter.com/TransCanada

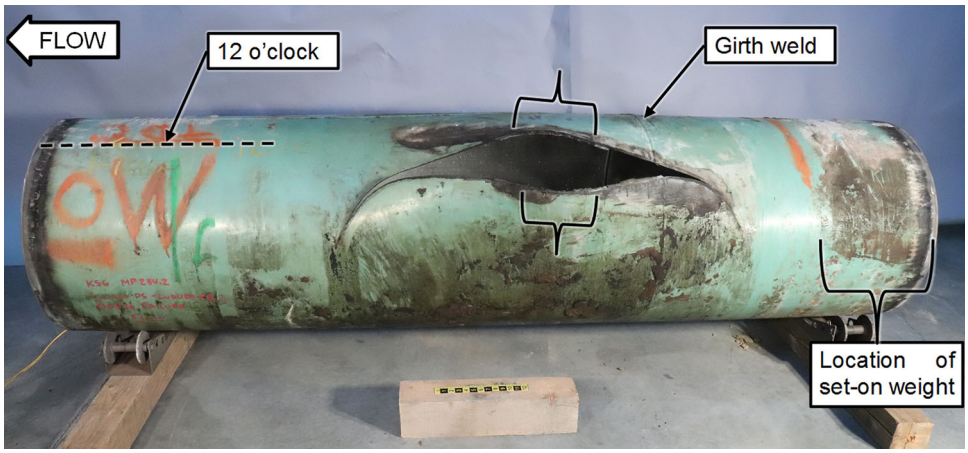

Fig. 2 Pipeline piece as received. Unlabeled brackets indicate the fatigue region near the middle of the rupture

Procedure

During the on-scene examination and documentation of the rupture, the section of pipe with the rupture was cut from the remainder of the line, and the fracture surfaces were cleaned using oil-dissolving solvents and a nylon brush. To prepare for shipping, the fracture surfaces were sprayed with a light oil and then brush-coated with Tectyl 506 (Daubert Chemical Company, Chicago, Illinois) wax-based, solvent cutback corrosion preventive compound. The fracture surfaces were then covered with a flexible hose that had been cut longitudinally on one side to be fitted over each fracture surface. The ruptured portion of the pipe section was wrapped in plastic, and the ends were capped. The section was then strapped in a crate for shipping. A piece cut from the lower end of a set-on weight located near the rupture was also secured in the crate.

Upon receipt by the NTSB Materials Laboratory, the components were photographed using a Canon EOS Rebel SL2 camera as they were removed from the crate and as packaging was removed. Oily soil deposits on the pipe surfaces away from the rupture were cleaned using a brush or cloth dipped in a solution of Alconox detergent and water. On the fracture surface and adjacent damaged exterior surface, acetone and mineral oil were used with a soft-bristle brush to remove oily deposits and the Tectyl 506. The solvents were initially ineffective at the cool temperatures in the minimally heated high-bay area where the cleaning was taking place, and eventually heat was applied using a heat gun to facilitate the removal of the oily deposits and the Tectyl 506.

The cleaned surfaces were then photographed and scanned using a FARO Technologies Incorporated EDGE FaroArm coordinate measurement device fitted with a Laser Line Probe HD. The 3-D point cloud data representing the exterior surface of the pipe was acquired and processed using 3D Systems Geomagic Studio 2014 software. Fluorescent magnetic particle inspection (MPI) was conducted on the pipe exterior in the areas where coating was missing or removed. After the MPI inspection was

complete, longitudinal and shear wave ultrasonic testing was completed from the interior surface to inspect for cracks, and an ultrasonic gauge was used to measure wall thickness.

Next, a rectangular piece of the pipe wall encompassing the rupture was cut from the rest of the piece, and additional longitudinal cuts were made intersecting the ends of the rupture to separate the two sides of the fracture. The exterior and interior sides of each piece were then scanned using the EDGE FaroArm with Laser Line Probe, and the resulting data, which was acquired in Geomagic Studio, was further analyzed using the thickness plot tool in 3D Systems Geomagic Control X software.

As cuts were made to facilitate further examinations of the fracture surface and areas of damage on the exterior surface adjacent to the fracture, surfaces were cleaned using a solution of Alconox detergent and water with a soft-bristle brush and rinsed with ethanol. The pieces were examined under optical magnification using a Nikon SMZ1500 optical stereomicroscope. In addition to photodocumentation, magnified optical images of the fracture surfaces and other areas of interest identified during the examination were captured using a Keyence VHX-5000 digital microscope. The fracture surfaces and adjacent areas of damage on the exterior surface were also examined using a Zeiss Auriga CrossBeam field-emission scanning electron microscope (SEM) fitted with a ThermoFisher Scientific UltraDry energy-dispersive x-ray spectroscopy (EDS) detector. Metallographic specimens were examined using a Zeiss Axio Observer Z1m optical metallograph followed by SEM imaging and EDS analysis that was conducted after sputter coating the samples with a gold/palladium alloy to prevent charging from the nonconductive mount material.

Samples were cut from the pipe wall opposite the longitudinal seam for tensile and Charpy impact tests and chemical analysis completed by Lehigh Testing Laboratories in New Castle, Delaware. Three room-temperature tensile tests were conducted using subsize round specimens with a ¼-in.-diameter (6.4-mm-diameter) cross section in the gage length and oriented in the transverse direction. Fifteen Charpy impact tests were conducted at five different temperatures using subsize specimens with a 6.7-mm-by-10-mm cross section oriented in the transverse direction (notch pointing parallel to the longitudinal axis of the pipe).

Findings

Near the middle of the fish mouth-shaped rupture, the fracture occurred in a plane perpendicular to the hoop direction in a region with curving crack arrest features and a curving boundary, features consistent with fatigue fracture (Fig. 3). The fatigue region was located near the top of the pipe approximately 10.75 in. (27.3 cm) circumferentially away from the longitudinal seam and 12.8 to 18.3 in. (32.5 to 46.5 cm) downstream of a girth weld. The length of the fatigue region at the exterior surface was 5.52 in. (14.0 cm) long and extended through the pipe wall thickness along 1.95 in. (4.95 cm) at the interior surface. The remainder of the fracture beyond the fatigue region occurred on slant angles and was associated with necking deformation, features consistent with ductile overstress fracture.

The exterior surface adjacent to the fatigue region had a shallow smooth depression consistent with heavy sliding contact with an object with a convex curved surface (Fig. 4). Based on a differential wall thickness measurement, the groove depth was 0.0196 in. (0.498 mm) near the middle of the fatigue region. The fracture adjacent to the sliding contact damage extended at a shallow angle relative to the exterior surface up to a depth of 0.098 in. (2.5 mm) (Fig. 5). Ratchet marks were observed on the fracture surface of the near-surface cracks radiating from the exterior surface, and the near-surface crack boundary had multiple curving segments, indicating crack initiation from multiple origins at the exterior surface. At the boundary of the near-surface crack, the fracture plane changed to a plane perpendicular to the hoop direction. Separate ratchet marks radiated from the near-surface crack boundary, consistent with fatigue initiation from multiple origins along the near-surface crack boundary.

SEM examination of the fatigue region revealed transgranular fracture features with river markings consistent with a cleavage or quasi-cleavage overstress fracture in the near-surface crack region (Fig. 6). Transgranular fracture features consistent with fatigue were observed emanating from the near-surface cracks. Multiple prominent crack arrest lines were observed, but fine fracture features were obliterated by post-fracture abrasion damage or were obscured by carbon-based deposits. Beyond the fatigue region, dimple features associated with micro void coalescence were observed in the ductile overstress portion of the rupture.

On the exterior surface of the pipe, areas of missing coating and sliding contact marks were observed on both sides of the fracture both upstream and downstream of the origin area. The greatest quantity of sliding contact marks was observed near the girth weld upstream of the fatigue region, where 14 distinct marks were observed and labeled with letters (Fig. 7). The sliding contact marks consisted of partially overlapping round-bottom grooves aligned mostly parallel to the longitudinal axis of the pipe. Three of the sliding contact marks were oriented at approximately 45 degrees relative to the longitudinal axis and had continuity across the longitudinal marks, indicating that they had been

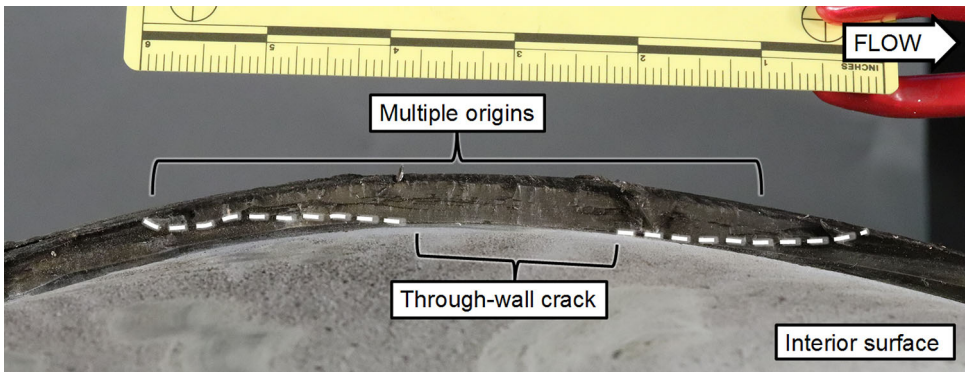

Fig. 3 Closer view of the fatigue region on the left fracture face

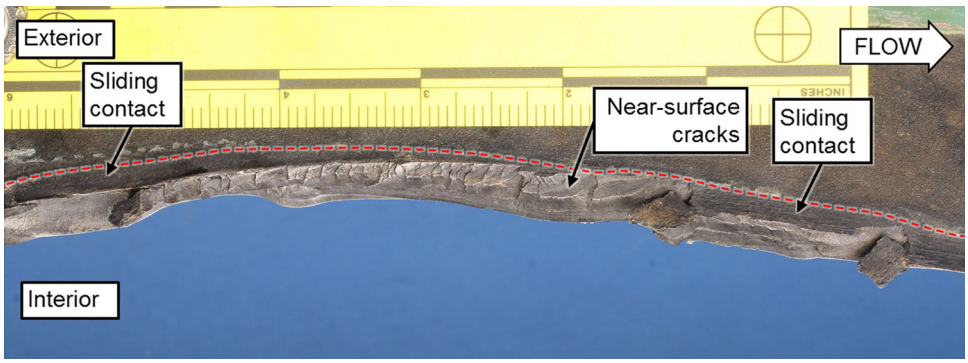

Fig. 4 Oblique view of the fatigue region on the left fracture face showing sliding contact damage bounded by the dashed line on the exterior surface adjacent to the fracture

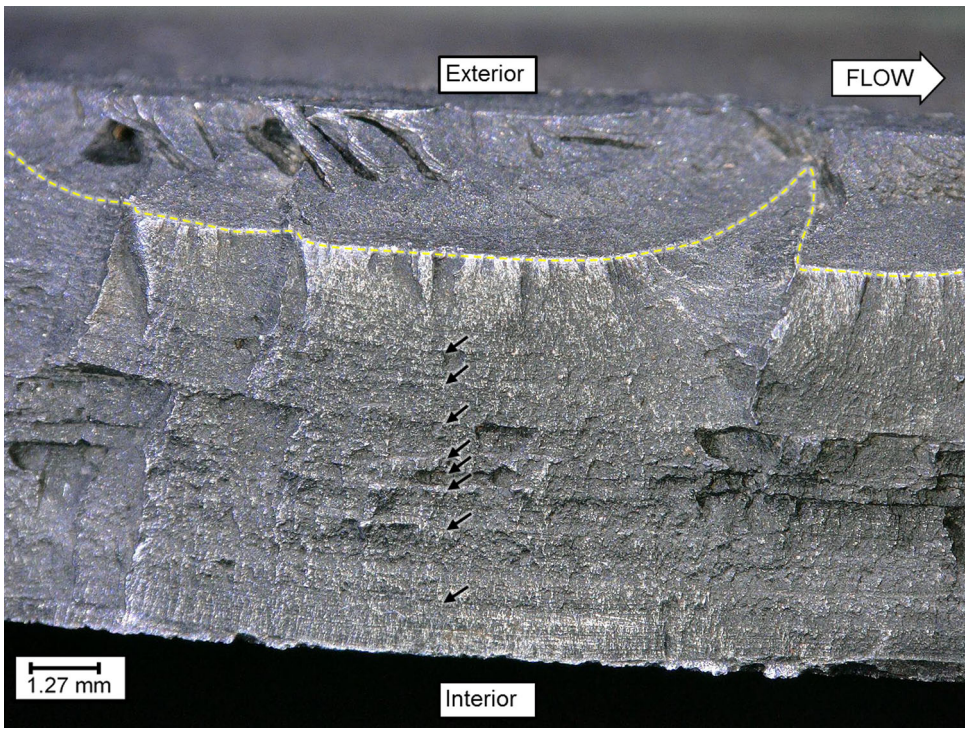

Fig. 5 Fatigue region in an area of through-wall penetration. A dashed line indicates the near-surface crack boundary, and unlabeled arrows indicate prominent fatigue crack arrest lines

made after the longitudinal marks. Coating material was present intermixed with the sliding contact marks, and many edges of the remaining coating adjacent to individual contact marks were curled and rounded consistent with sliding contact deformation. Additionally, linear abrasions aligned with the contact marks were observed on the surface of intact coating material at the downstream end of the area exhibiting sliding contact marks.

A thickness map generated from a 3D scan of the pipe piece provided another way to visualize the damage (Fig. 8). In the thickness plot, deeper grooves appear red. The thickness plot also shows evidence of necking adjacent to the fracture and a magenta-colored edge associated with the slant-plane fracture. Dark green areas of the plot show some areas of the pipe with intact coating and the weld bead associated with the girth weld.

Many of the grooves had crack indications detected by MPI. Networks of crack indications and segments of linear indications were observed in the sliding contact areas. However, many of the indications could be associated with lips of overlapped metal in the deformed metal surface and were not necessarily associated with a crack. The areas where indications were brighter and more linear were bracketed with yellow wax marker on the pipe surface (Fig. 7).

After the 3D scans of the damage were complete, a cut was made in the circumferential plane through the area of sliding contact, which revealed the groove profiles. The radii of curvature at 5 of the groove bottoms were measured using the Keyence VHX-5000 microscope by fitting a circle to the groove profile in the cut plane (Fig. 9). The measured radius of curvature ranged from 0.085 to 0.233 in. (2.16 to 5.92 mm) with an average of 0.129 in. (3.28 mm).

The exterior surface downstream of the circumferential cut was cleaned with a soft-bristle brush using a solution of Alconox and water and rinsed with water followed by ethanol. In the area of sliding contact grooves, portions of the surface within the grooves appeared lighter gray compared to the adjacent surfaces (Fig. 10). A partially opened longitudinal crack-like feature was also observed in one of the sliding contact grooves.

The piece shown in Fig. 10 was sectioned for SEM, EDS, and metallography including a transverse cut through the partially opened crack-like feature. SEM examination of the crack-like feature revealed fracture features that were visible when viewed through the crack opening (Fig. 11). Transgranular fracture features with tear ridges were observed, indicative of quasi-cleavage features consistent with overstress fracture. During the SEM examination, the exterior surface of the sectioned piece was also analyzed using EDS. The spectra for the lighter

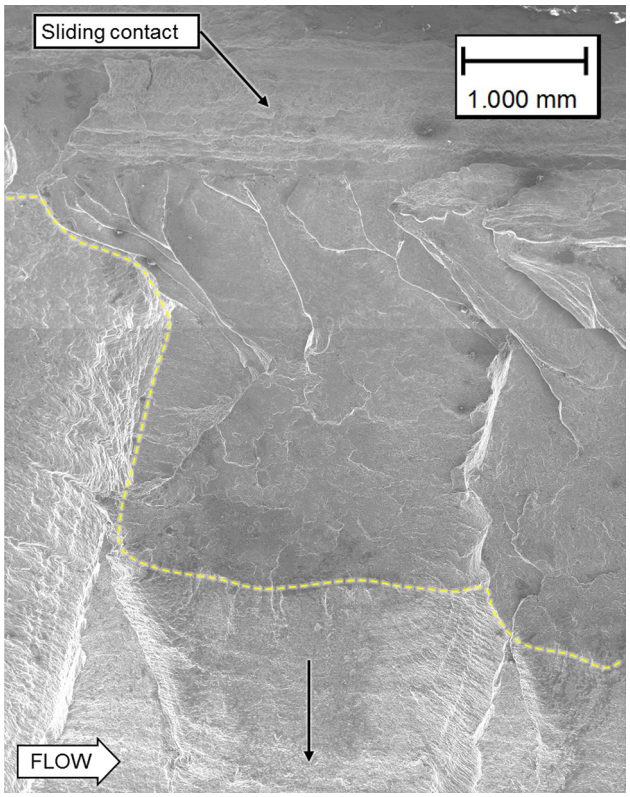

Fig. 6 SEM image of sliding contact features, near-surface cracks, and fatigue features. A dashed line indicates the near-surface crack boundary, and an unlabeled arrow indicates the fatigue crack propagation direction

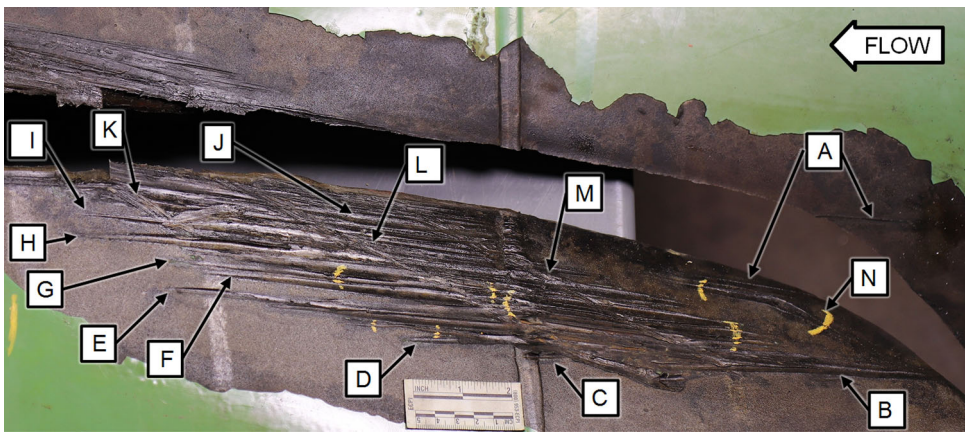

Fig. 7 Sliding contact marks on the exterior surface upstream of the fatigue region

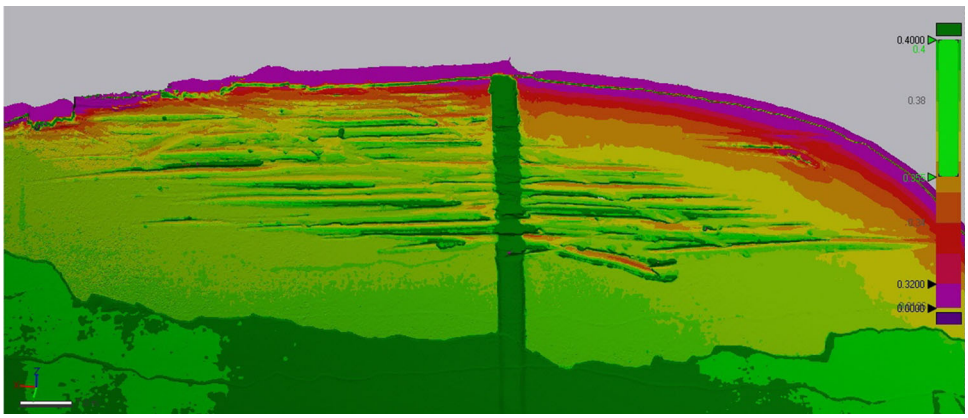

Fig. 8 Thickness contour plot in the area of sliding contact marks (Color figure online)

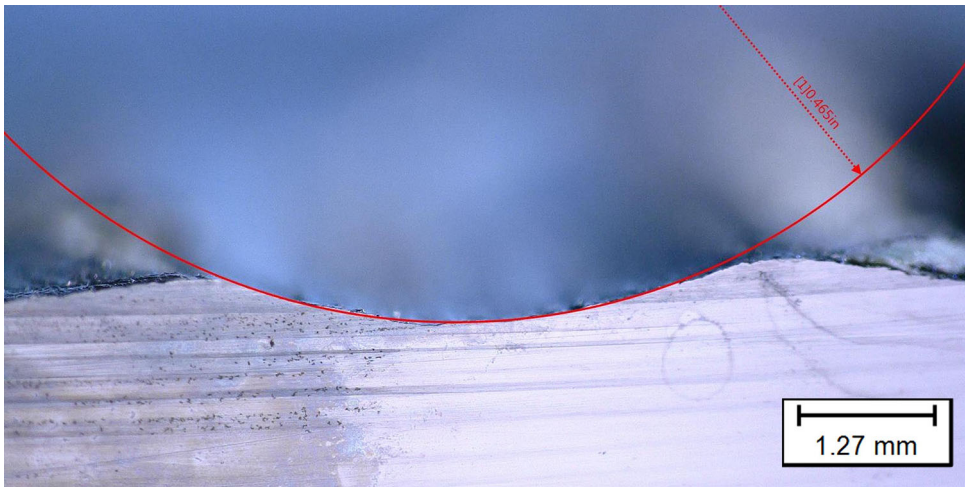

Fig. 9 Sliding contact groove radius measurements in the transverse plane

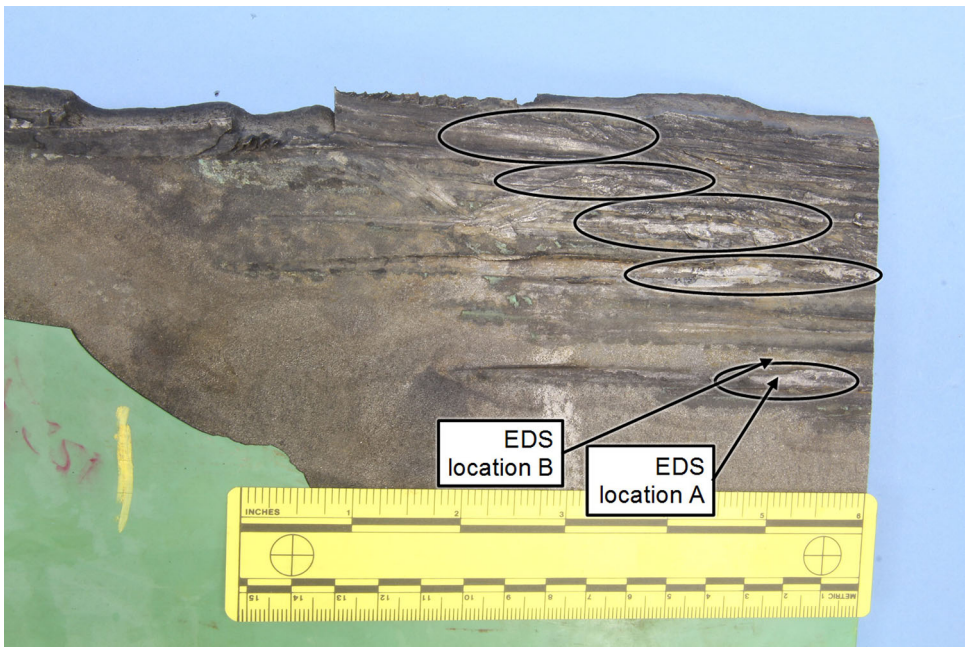

Fig. 10 Area of sliding contact marks after sectioning and cleaning. Areas of lighter gray material with higher chromium content relative to the pipe material are indicated

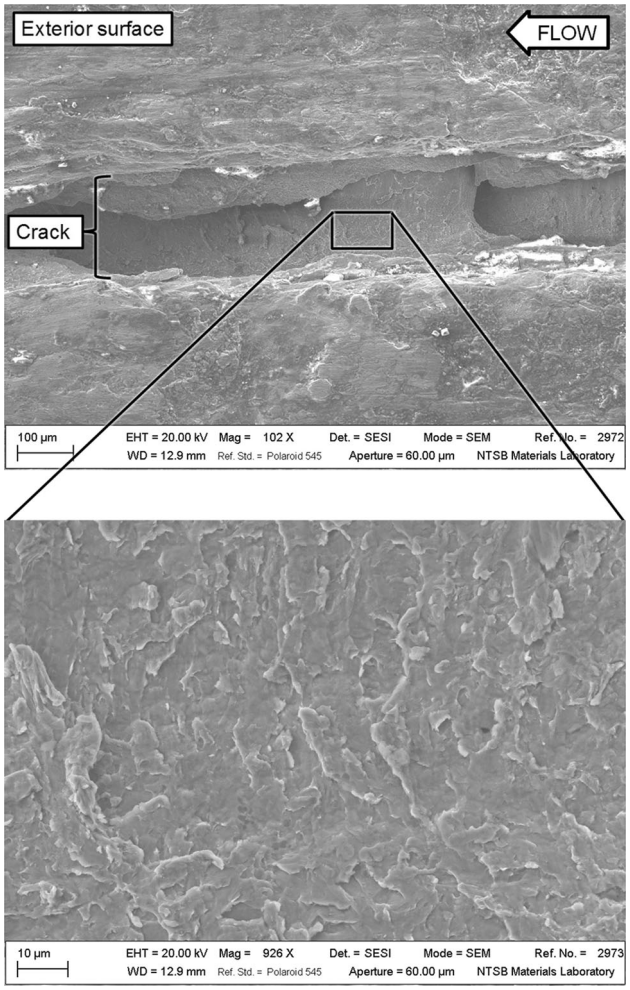

Fig. 11 Fracture features associated with a partially opened longitudinal crack observed in one of the sliding contact grooves

gray areas shown circled in Fig. 10 had relatively higher chromium peaks compared to the spectra obtained from the adjacent undisturbed pipe wall surfaces.

Metallographic samples were prepared in cross sections in the circumferential plane through the sliding contact grooves intersecting several of the lighter gray areas noted in Fig. 10. After etching with nital, a distinct layer of material that etched differently relative to the underlying pipe material was observed at the bottom of several grooves (Fig. 12). The metallographic samples were then coated with a gold/palladium alloy to prevent charging from the nonconductive metallurgical mounting material during a subsequent SEM examination and EDS analysis. EDS spectra were obtained from the surface layer and from the underlying pipe material and are shown overlayed for comparison (Fig. 13). Both spectra had high peaks of iron with smaller peaks of manganese and silicon consistent with low-alloy steel. However, the spectrum for the surface layer (shown in yellow) had a small chromium peak that

Fig. 12 Metallographic section through one of the grooves showing metal deposited on the surface as indicated with an unlabeled bracket (etched with 4% nital)

was mostly absent from the spectrum for the underlying pipe material (outlined in red).

The surface layer was further analyzed using EDS mapping by element. Distinct differences between the surface layer and the underlying pipe metal were observed in the maps for chromium and manganese (Fig. 14). The surface layer was consistently associated with higher counts for the chromium peak relative to the underlying material. In the map for manganese, bright spots associated with manganese-rich particles (likely manganese sulfide stringers) were observed only within the surface layer.

Mechanical properties including room-temperature tensile yield strength, ultimate strength, and elongation were determined for the pipe material. Additionally, Charpy impact energies were determined at five temperatures ranging from −100 to 212°F (−73 to 100°C). The measured mechanical properties all satisfied the requirements for steel manufactured to API 5L grade X70 PSL2 specifications. Chemical composition was also determined and was found to be within allowable ranges for the specified material.

Wall thickness was measured using a ball-flat micrometer at an undeformed area of the pipe wall within the ruptured segment, and results showed a thickness value that was within the allowable range for the specified nominal wall thickness. Thickness measurements of undamaged areas using an ultrasonic gauge and 3D thickness plots also showed wall thickness values within the allowable range.

Discussion

The pipe ruptured due to fatigue cracks that initiated from near-surface cracks associated with damage on the exterior surface of the pipe. The damage consisted of sliding contact marks including grooves associated with heavy contact

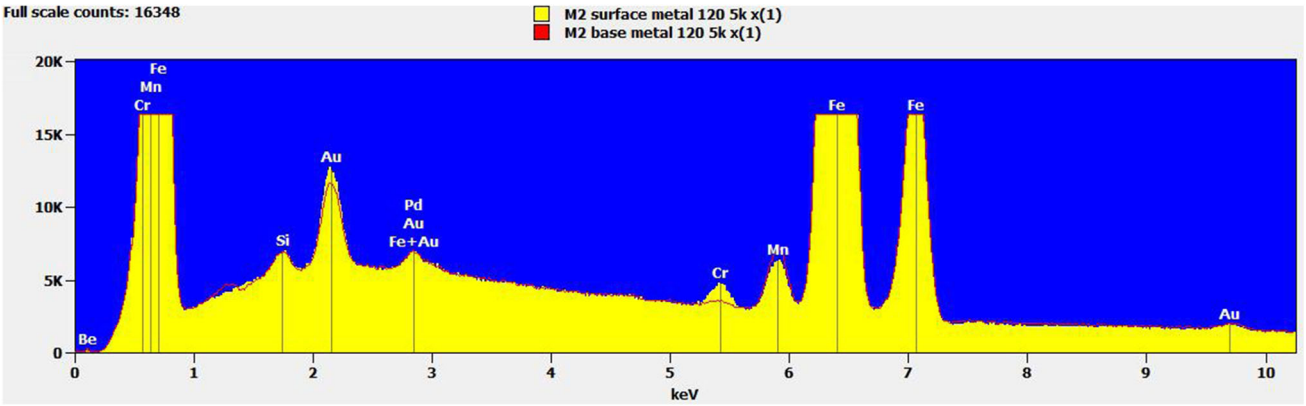

Fig. 13 EDS spectra of the gold palladium-coated metallographic section showing the deposited surface material spectrum in yellow, and the underlying pipe material spectrum outlined in red (Color figure online)

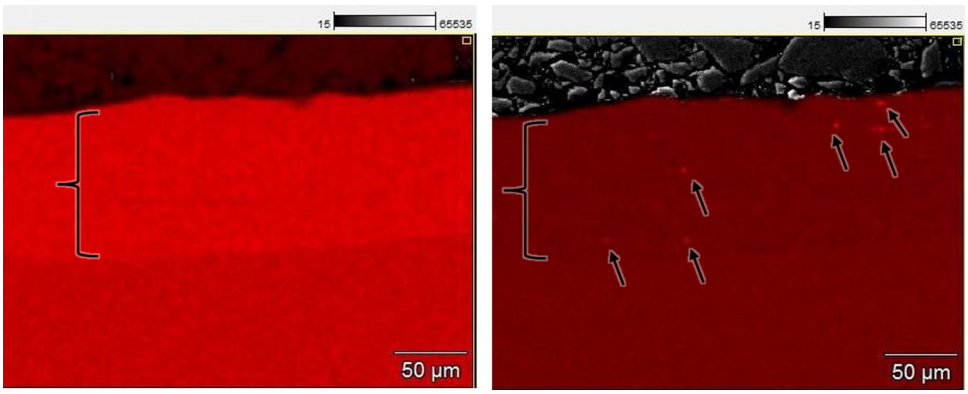

Fig. 14 EDS map of the deposited metal layer (indicated with unlabeled brackets) showing a layer of elevated chromium counts (left map) and particles with high manganese counts (unlabeled arrows in the right map) distinctly associated with the deposited layer

with another object. The contact pressures were substantial enough to locally deform the pipe metal to form the groove and cause near-surface cracks to develop within the damaged areas. The fatigue cracks then initiated and propagated from the near-surface cracks during subsequent pipeline operations.

The location of the coating damage patterns, the damage at the top of the pipe extending across the girth weld, the shape of the grooves, and transferred metal within the grooves provided clues to the source of the damage. The coating had abrasions and deformation associated with sliding contact, indicating the damage occurred after the pipe had been coated. Since the damage extended across the girth weld, the damage occurred after the pipe sections had been welded, and damage only to the top of the pipe is most likely to occur after a pipe is positioned in the trench. The grooves had rounded bottom profiles, and material from the contacting object had been transferred to the pipe surface within the grooves. Relative to the pipe steel, the transferred material had a higher chromium content and appeared to contain larger manganese sulfide particles. The overall geometry of the damage and transferred steel in the grooves indicated the pipe was likely contacted by a steel component from a construction vehicle. Since the rupture was located in a remote area with no record of heavy equipment activity in the time since construction and given the relatively low total time in service for the pipeline, the damage likely occurred during original construction. While no pipe damage or other equipment complications were documented in available construction records for the ruptured pipe segment, the PHMSA failure investigation report noted "the location was wet and muddy, the weather was cold and windy, and working conditions were very difficult" based on inspection records from days the ruptured segment was constructed.

As documented in the PHMSA failure investigation report, the failed segment passed a post-construction hydrostatic pressure test in June 2009. Several caliper in-line inspection (ILI) tools, used to detect geometric anomalies such as ovalization or dents, were passed through the damaged segment in the time since construction, and no actionable anomalies were detected at the rupture location. Two magnetic flux leakage ILI tools, used to detect changes in wall thickness, were also passed through the segment, and neither tool detected metal loss exceeding 10% of the wall thickness within 500 feet (152

m) of the rupture location. A Direct Current Voltage Gradient survey, which is used to detect exposed pipe wall surfaces from coating damage, was conducted to detect changes in current flow associated with the cathodic protection, and no readings requiring action were detected at the rupture location.

Conclusion

Both the NTSB pipeline accident brief and the PHMSA failure investigation report determined the accident likely resulted from mechanical damage that was sustained during pipeline construction. The damaged segment survived the post-construction hydraulic test, and the damage was not detected during subsequent pipeline inspections until the pipeline ruptured from a fatigue crack that initiated from near-surface cracks associated with the mechanical damage. The PHMSA failure investigation report concludes that it should be assumed that similar damage, which can be detected using existing ILI technology, could be sustained at any time throughout the lifetime of the pipeline, and implementation of more conservative assessment intervals would improve the probability of detection prior to failure.

Acknowledgments In accordance with Title 5 Code of Federal Regulations §2635.807(b)(2), the views expressed in this article do not necessarily represent the views of the National Transportation Safety Board or the United States. The authors acknowledge contributions to the investigation by Brian Pierzina who was the PHMSA Principal Investigator and Kalu Kelly Emeaba who was the NTSB Investigator in Charge. Additionally, the authors recognize contributions to the laboratory examination from Ed Komarnicki (NTSB), Bruce Dupius (TransCanada), Derek Chen (TransCanada), Darren Lemmerman (PHMSA), and Jennifer Philopoulos (Transportation Safety Board of Canada). The authors also appreciate consultation provided by Benjamin Andrews, Geologist and Curator of Rocks and Ores at the Smithsonian National Museum of Natural History.

References

1. B.E. Pierzina, *Failure Investigation Report: Material Failure—Mechanical Damage from Original Construction—TC Oil Pipeline Operations Inc*. (U.S. Department of Transportation Pipeline and Hazardous Safety Administration, Washington, D.C., 2018)
2. Pipeline Accident Brief, TransCanada Corporation Pipeline (Keystone Pipeline) Rupture, Amherst, South Dakota, PAB-18/01, National Transportation Safety Board (2018)
3. M.R. Fox, A.V. Lamm, Accident Docket PLD18LR001, Materials Laboratory Factual Report 18-017, National Transportation Safety Board (2018)
4. API Specification 5L, *Specification for Line Pipe*, 43rd edn. (American Petroleum Institute, Washington, D.C., 2004)